Hindawi Publishing Corporation
EURASIP Journal on Advances in Signal Processing
Volume 2008, Article ID 241069, 14 pages
doi:10.1155/2008/241069

Research Article

A Markov Model for Dynamic Behavior of ToA-Based Ranging in Indoor Localization

Mohammad Heidari and Kaveh Pahlavan

Center for Wireless Information Network Studies, Electrical and Computer Engineering, Worcester Polytechnic Institute, 100 Institute Road, Worcester, MA 01609, USA

Correspondence should be addressed to Mohammad Heidari, mheidari@wpi.edu

Received 28 February 2007; Revised 27 July 2007; Accepted 26 October 2007

Recommended by Sinan Gezici

The existence of undetected direct path (UDP) conditions causes occurrence of unexpected large random ranging errors which pose a serious challenge to precise indoor localization using time of arrival (ToA). Therefore, analysis of the behavior of the ranging error is essential for the design of precise ToA-based indoor localization systems. In this paper, we propose a novel analytical framework for the analysis of the dynamic spatial variations of ranging error observed by a mobile user based on an application of Markov chain. The model relegates the behavior of ranging error into four main categories associated with four states of the Markov process. The parameters of distributions of ranging error in each Markov state are extracted from empirical data collected from a measurement calibrated ray tracing (RT) algorithm simulating a typical office environment. The analytical derivation of parameters of the Markov model employs the existing path loss models for the first detected path and total multipath received power in the same office environment. Results of simulated errors from the Markov model and actual errors from empirical data show close agreement.

1. INTRODUCTION

Recently, indoor localization technology has attracted significant attention, and a number of commercial and military applications are emerging in this field [1]. Indoor channel environments suffer from severe multipath phenomena, creating a need for novel approaches in design and development of systems operating in these environments [2, 3]. Precise indoor localization systems are designed based on range measurements from time of arrival (ToA) of the direct path (DP) between transmitter and receiver, which is severely challenged by unexpected large errors [4]. Therefore, the ranging error modeling is essential in design of precise ToA-based indoor localization systems.

There are empirical indoor radio propagation channel models available in the literature aiming primarily at telecommunication applications [5–8]. These models were designed prior to the understanding of the indoor localization problem, and hence they did not concern the behavior of ranging error in indoor environment. Therefore, they do not provide a close approximation to the empirical observations of the ranging error [9]. More recently, indoor radio propagation channel models designed for ultrawide bandwidth (UWB) communications, specifically the work of IEEE 802.15.3 and IEEE 802.15.4*a*, have paid indirect attention to the indoor localization problem [10–15], and recent research studies propose UWB measurement system to obtain high-accuracy localization systems [16, 17]. However, these indirect models have not paid special attention to the occurrence of undetected direct path (UDP) conditions, which is the main cause of large errors in ranging estimate. The first direct empirical model for ranging error is reported in [9, 18, 19]. These new direct models, however, do not address the spatial correlation of the ranging error behavior observed by a mobile user.

This paper presents a new methodology and a framework for modeling and simulation of dynamic variations of ranging error observed by a mobile user based on an application of Markov chain. Markov chains, and particularly hidden Markov models (HMMs), are widely used in the

telecommunication field. In [20], it is proposed to exploit HMM in radar target detection. In [21], HMM is employed along with Bayesian algorithms to provide a reliable estimate of the location of the mobile terminal and to trace it. Furthermore, in [22], HMM is used along with tracking algorithms to provide a footmark of the nonline-of-sight conditions, present a reliable estimate of the location of the mobile terminal, and track it.

We categorize the ranging error into four different classes and present clarifications as to the statistical occurrence of each class of ranging errors. Furthermore, we provide distributions to model typical values of ranging error observed in each class of receiver locations. Next, we link each class of ranging errors to a state of a Markov process which can be used for the simulation of spatial behavior of the class of ranging errors for a mobile user randomly traveling in a building. Finally, we provide a method to statistically extract the average probabilities of residing in a certain state for the building under study. The presented model for dynamic behavior of ranging error is essential for the design and performance evaluation of tracking capabilities of the proposed algorithms for indoor localization. The parameters of the Markov model are analytically derived from the results of the UWB measurement conducted on the third floor of the Atwater Kent laboratories (AK Labs) at Worcester Polytechnic Institute (WPI). The parameters of distributions of ranging error in each Markov state are extracted from empirical data collected from a measurement calibrated ray tracing (RT) algorithm simulating the same office environment. The commonly used RT software, previously used in literature for communication purposes [23, 24], provides the radio propagation of the indoor environment in which reflection and transmission are the dominant mechanisms. It has been shown that the existing RT software can be a useful and practical simulation tool to assess the behavior of ranging error in indoor environments [9].

The paper is organized as follows. Section 2 summarizes the background of ranging error modeling and classification of ranging error, while Section 3 introduces a new framework for the classification of ranging error observed in indoor environment and presents the concept of state probability. Section 4 discusses the principles of Markov model, analytical derivation of the parameters of the Markov chain, and modeling of the state probabilities. Finally, Section 5 summarizes the results and comments on the outcome of the simulation.

2. FOUR CLASSES OF RANGING ERRORS

2.1. Background

In general, it has been observed that wireless channel consists of paths arriving in clusters. The most popular method to reflect this behavior on the channel response is based on Saleh-Valenzuela model [5], in which the discrete multipath indoor channel impulse response (CIR) can be characterized as

$$h(t) = X\sum_{l=1}^{L}\sum_{k=1}^{K}\alpha_{k,l}e^{j\phi_{k,l}}\delta\left(t - T_l - \tau_{k,l}\right), \tag{1}$$

where $\{T_l\}$ represents the delay of the lth cluster, $\{\alpha_{k,l}\}$, $\{\phi_{k,l}\}$, and $\{\tau_{k,l}\}$ represent tap weight, phase, and delay of the kth multipath component relative to the lth cluster arrival time (T_l), respectively, and X represents the log-normal shadowing [10, 12]. The tap weights, $\{\alpha_{k,l}\}$, are determined based on practical path loss exponents and signal loss of different building materials for reflection and transmission mechanisms in indoor environment [25]. The CIR then consists of $\{\alpha_{k,l}\}$ which are within the dynamic range of the system. In this article, we use (1), previously used in IEEE 802.15.3*a*, to model the behavior of channel since it highlights the importance of cluster-based arrival of paths. However, a more sophisticated cluster-based model can be used to fully model the behavior of the wireless channel. The interested reader can refer to [11, 15] for more detailed modeling and description of UWB channels.

The CIR is usually referred to as *infinite-bandwidth channel profile* since with infinite bandwidth the receiver could theoretically acquire every detectable path. Let $\alpha_{\mathrm{DP}} = \alpha_{1,1}$ and $\tau_{\mathrm{DP}} = \tau_{1,1}$ represent the amplitude and ToA of the DP component, respectively. In ToA-based positioning systems, the distance between the antenna pair is obtained using $d = \tau_{\mathrm{DP}} \times c$, where c represents the speed of light. The range estimate is determined using $\hat{d} = \tau_{\mathrm{FDP}} \times c$, where τ_{FDP} represents the ToA of the first detected path (FDP) of the channel profile within the dynamic range of the system. The distance measurement or ranging error in such systems is then defined as $\varepsilon = \hat{d} - d$ [9, 18].

In practice, however, the limited bandwidth of the localization system results in arriving paths with pulse shapes, which is referred to as channel profile and can be represented by

$$h(t) = X\sum_{l=1}^{L}\sum_{k=1}^{K}\alpha_{k,l}s\left(t - T_l - \tau_{k,l}\right), \tag{2}$$

where s represents the time-domain pulse shape of the filter. In practice, Hanning and raised-cosine filters are widely used in today localization domain. As a result of filtering the CIR, sidelobes of each pulse shape respective to each path can be constructively or destructively combined to each other and form different peaks which consequently limit the accuracy of the ranging process.

In the past decade, empirical results from software simulation using RT [9], wideband [3], and UWB [18] measurements of the indoor radio propagation have revealed the occurrence of a wide variety of ranging errors. In the most common classification of the receiver location, the sight condition between the transmitter and the receiver categorizes the receiver location and the ranging error associated with it into two main classes of line-of-sight (LoS) and nonline-of-sight (NLoS) conditions. However, further investigation reported that depending on the relative location of the transmitter and receiver and their position with respect to the blocking objects, that is, large metallic objects, these ranging errors can be further divided into four main categories of detected direct paths (DDPs), natural undetected direct paths (NUDPs), shadowed undetected direct paths (SUDPs), and no coverage (NC) [4, 9, 26, 27]. The focus of this research is on the

ranging error modeling of LoS/DDP, NUDP, and SUDP and on modeling the dynamic behavior of ranging error observed by mobile client in indoor environment.

2.2. Ranging error classification based on power

The receiver location classification is mainly accomplished by means of power. In such classifications, the class of ranging errors associated with each receiver location can be defined according to the power of the DP component and the total received power given by

$$P_{\mathrm{DP}} = 20\log_{10}(|\alpha_{\mathrm{DP}}|),$$
$$P_{\mathrm{tot}} = 10\log_{10}\left(\sum_{l=1}^{L}\sum_{k=1}^{K}|\alpha_{k,l}|^2\right) \quad (3)$$

as well as blocking condition λ_i, which is a binary index to indicate the blockage of DP and its adjacent components by an obstructive object. In this paper, it is assumed that for the specified locations of the transmitter and receiver, the true value of λ_i is known, where $\lambda_i = 0$ represents a channel profile which is not blocked and $\lambda_i = 1$ represents a channel profile which is blocked by an obstructive object.

In DDP class of receiver locations, which is indeed a subclass of LoS, $\lambda_i = 0$, $P_{\mathrm{DP}} > \eta$, and $P_{\mathrm{tot}} > \eta$, in which η represents the detection threshold and it is dependent on the measurement noise of the system. Fixing the transmitter power at a regulated level, η can be related to the dynamic range of the system. However, increasing the dynamic range of the system, that is, decreasing η, raises the likelihood of the DP component to be detected at the receiver side, but it also increases the probability of detecting a noise term (or a sidelobe peak) as the DP component, that is, a false alarm [28]. Efficient selection of the proper value of η can improve the accuracy of the localization system [29]. Typical values of η are 5∼10 dB above the measurement noise present in indoor environment. In DDP conditions, $\tau_{\mathrm{FDP}} \approx \tau_{\mathrm{DP}} = \tau_{1,1}$ and $\varepsilon = (\tau_{\mathrm{FDP}} - \tau_{1,1}) \times c$ result in insignificant ranging error associated with the ToA measurement given by

$$f_{\varepsilon_{\mathrm{DDP}}}(\varepsilon) = f^{\mathbf{M}}(\varepsilon), \quad (4)$$

where $f^{\mathbf{M}}$ represents the multipath-induced errors which are considered as the main source of ranging errors in LoS/DDP class.

In NUDP class of receiver locations, $\lambda_i = 0$ and $P_{\mathrm{tot}} > \eta$, but $P_{\mathrm{DP}} < \eta$, resulting in $\tau_{\mathrm{FDP}} = \tau_{1,k,k\neq 1}$, which indicates that the DP component is not within the dynamic range of the system, and hence it cannot be detected, but a neighboring path from the first cluster was detected as the FDP. Consequently, $\varepsilon = (\tau_{\mathrm{FDP}} - \tau_{1,1}) \times c$ is in the order of ray arrival rate defined in the CIR system model presented in (2). It has been shown that NUDP ranging errors are small and occur in small bursts [4]. The gradual weakening of the DP component due to loss of power from reflection and transmission mechanisms suggests that by moving further from the transmitter at a certain break-point distance, the power of the DP component, P_{DP}, falls below the detection threshold, that is, not within the dynamic range of the system, and consequently the receiver exits DDP condition and enters NUDP condition. Similar to DDP class of receiver locations, in NUDP regions, the error is given by

$$f_{\varepsilon_{\mathrm{NUDP}}}(\varepsilon) = f^{\mathbf{M+NUDP}}(\varepsilon), \quad (5)$$

where $f^{\mathbf{M+NUDP}}$ indicates that the multipath and loss of DP component are the main sources of ranging errors.

Contrary to the above states, in SUDP class of receiver locations, the attenuation of the multipath components results in very weak paths regarding the first cluster, that is, channel profiles with *soft onset* CIR [11, 30], which shift the strongest component to the middle of the CIR. Consequently, for SUDP class of receiver locations, $P_{\mathrm{DP}} < \eta$ and $P_{\mathrm{tot}} > \eta$, but $\lambda_i = 1$ denoting that the receiver location is blocked by a metallic object. In such scenarios, $\tau_{\mathrm{FDP}} = \tau_{i,j,i\neq 1}$, indicating the blockage of the first cluster and the fact that the second cluster is detected instead, resulting in FDP component being either the first or one of the following paths of the second cluster. Consequently, $\varepsilon = (\tau_{\mathrm{FDP}} - \tau_{1,1}) \times c$ is in the order of cluster arrival rate defined in the CIR system model. Results of extensive UWB measurement and simulation in indoor environments confirm the occurrence of unexpected large ranging errors associated with SUDP condition observed in indoor environment [3, 9, 18, 19]. For SUDP regions,

$$f_{\varepsilon_{\mathrm{SUDP}}}(\varepsilon) = f^{\mathbf{M+NUDP+SUDP}}(\varepsilon), \quad (6)$$

where $f^{\mathbf{M+NUDP+SUDP}}$ indicates that multipath, loss of DP component, and blockage are the main sources of ranging errors.

Finally, for the last class of receiver locations, which is referred to as NC conditions, $P_{\mathrm{tot}} < \eta$ in which communication is not feasible and the receiver is out of range. Assuming that the mobile terminal resides in one of the UDP areas, by moving further from the transmitter at a certain break-point distance, the receiver transitions from UDP condition to NC condition. In NC condition, the range estimate is not available and ranging error is undefined.

Figure 1 illustrates the areas associated with the four classes of ranging errors on the third floor of AK Labs at WPI for the specified location of the transmitter. To determine the areas, we have used the measurement calibrated RT software previously used in [9] to generate comprehensive samples of CIR for different locations of the receiver in the building. The class of ranging errors associated with each receiver location is defined according to P_{DP} and P_{tot} given by (3) and the physical layout of the building, represented by λ_i. Increasing the distance of the antenna pair in indoor environment increases the probability of blockage of the DP component. In NUDP class of receiver locations, although the receiver location is not blocked by metallic objects, P_{DP} falls below the detection threshold η, and hence the receiver makes erroneous estimate of the distance of the antenna pair. In SUDP class of receiver locations, blockage of the DP component and its adjacent paths with a metallic object attenuates the DP component and its adjacent paths significantly, and hence the receiver makes an unexpectedly large ranging error by detecting another reflected path.

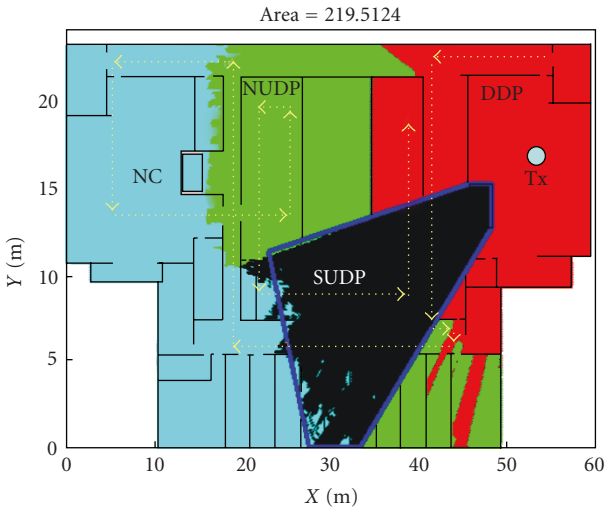

Figure 1: Indoor receiver classification simulation for a sample location of the transmitter. The location of the metallic chamber close to the transmitter causes lots of SUDP receiver locations.

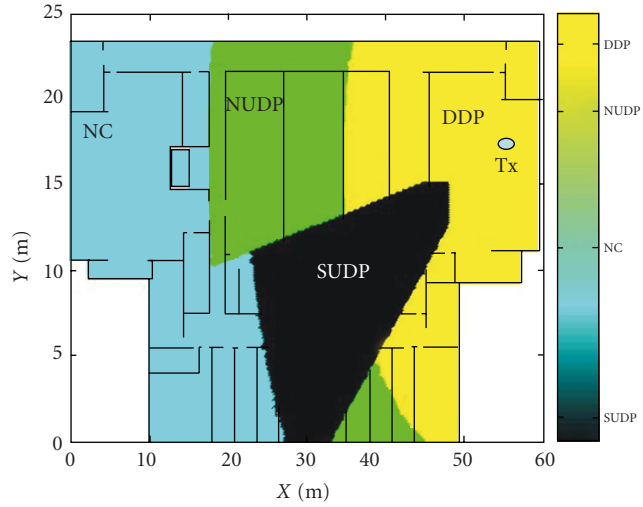

Figure 2: Indoor receiver classification for the same location of the transmitter based on infrastructure-distance-measurement (IDM) model.

3. RANGING ERROR CLASSIFICATION BASED ON DISTANCE

3.1. *Infrastructure-distance-measurement- (IDM-) based model*

The receiver location classification described above is very difficult to obtain as it is computationally tedious and time-consuming. Alternatively, to avoid the extensive simulation and/or measurement to categorize the receiver locations in a building, we have developed an infrastructure-distance-measurement-(IDM-) based model based on the realistic path loss models for indoor environment [9] to represent different classes of receiver locations and ranging errors associated with them. Assuming the knowledge of blockage condition, $\lambda_i(r)$, for each receiver location, the proposed model can be represented as follows:

$$\xi_i = \begin{cases} \text{DDP}: & d < d_1 \cap \lambda_i(r) = 0, \\ \text{NUDP}: & d_1 < d < d_2 \cap \lambda_i(r) = 0, \\ \text{SUDP}: & d < d_3 \cap \lambda_i(r) = 1, \\ \text{NC}: & \begin{cases} d > d_2 \cap \lambda_i(r) = 0, \\ d > d_3 \cap \lambda_i(r) = 1, \end{cases} \end{cases} \tag{7}$$

where ξ_i represents the class of receiver locations and d_1, d_2, and d_3 represent the distance break-point of DDP and NUDP regions, the distance break-point of NUDP and NC regions, and the distance break-point of SUDP and NC regions, respectively. The sample break-points are determined by extensive frequency measurements (sweeping frequency of 3–8 GHz with a sampling frequency of 1 MHz) conducted in the sample indoor environment [31] to be around 18 m, 35 m, and 30 m, respectively. The measurement setup has a sensitivity of −80 dBm representing the detection threshold [9, 32]. Altering the sensitivity of the measurement system, that is, the detection threshold and dynamic range of the system, as well as other parameters of the measurement will cause modifications in determination of the break-point distances [28]. However, such modifications are not in the scope of this article, and the reported break-point distances are determined using the above measurement setup.

To verify the validity of the proposed model, that is, IDM realization, we can compare it with RT simulation. Very close agreement between RT simulation and IDM realization of different categories is illustrated in Figure 2, which demonstrates the validity of the proposed IDM realization. The above model, however, represents the static classification of the receiver locations in indoor environments.

3.2. *Introduction to state probabilities*

Having defined the four classes of receiver locations and ranging errors, we can define the state probability of each state which is the average staying time of the mobile client in that state. Modeling the state probabilities enables us to predict the class of ranging errors that a mobile user observes traveling in indoor environment. It also helps in Markov chain initialization as it models the average probability of residing in a certain state. For each class of receiver locations, the state probability is defined as

$$P_z = P(\xi_i \in z) = \frac{\iint_{\xi_i \in z} dx\, dy}{\iint_{\xi_i \in M} dx\, dy}, \tag{8}$$

in which M represents the union set of receiver locations and $z \in \{\text{DDP}, \text{NUDP}, \text{SUDP}, \text{NC}\}$ represents the desired state.

The state probabilities, in general, are not easy to find analytically as they vary with the change of transmitter location and shape and details of the building. However, statistics of the state probabilities are easy to find and model by altering the location of the transmitter and modeling the result

of simulation. Using (7) to categorize the receiver locations into DDP, NUDP, SUDP, and NC for the same indoor environment described in Figure 2, we were able to compare the average SUDP state probability of the IDM realization and wideband measurement previously conducted in the same scenario. We observed that on average a random mobile client would expect to be in SUDP condition with probability of 8.9% according to IDM realization which is close to the reported value of 7.4% obtained from wideband measurement [9, 26].

Each state probability can be considered as a random variable. Knowing the statistics of the state probability for a certain state, we are able to define the cumulative distribution function (CDF) of the state probability. It follows that

$$F_{P_{\text{SUDP}}}(p_1) = P\{P_{\text{SUDP}} < p_1\}, \tag{9}$$

which discloses the receiver locations in which its state probability is less than a certain value p_1. Finally, the probability distribution function (PDF) can be defined as $f_{P_{\text{SUDP}}}(p_1) = \partial F_{P_{\text{SUDP}}}(p_1)/\partial p_1$. It is worth mentioning that $f_{P_{\text{SUDP}}}$ can be considered as a random variable modeling the distribution of SUDP state probability, which itself is limited to the interval $[0, 1)$. Therefore, the outcome of such distribution should be truncated to remain in $[0, 1)$ so as to ensure that state probabilities are within their limits.

4. DYNAMIC BEHAVIOR OF RANGING ERROR

A random mobile client in an indoor environment experiences switching among different classes of ranging errors, back and forth, as it keeps moving. Such spatial correlation and change of class can easily be modeled with Markov chains.

4.1. Ranging states of the Markov model

As the mobile client randomly travels in the building, as shown in Figure 1, depending on the region of movement, it experiences different classes of ranging errors. Using the four classes of ranging errors observed in separate areas of an indoor environment, we can construct a four-state first-degree Markov model to represent the dynamic behavior of ranging error observed by the mobile user. Random movement of the mobile user results in change of its observed class of ranging errors, with particular probabilities. The general Markov model representation for indoor positioning is described in Figure 3. Let the current receiver location, ξ_i in (7), embed the state of the mobile terminal ω_i, where ω_i is defined over a discrete set Z consisting of four different receiver location classes or states, $Z = \{\text{DDP}, \text{NUDP}, \text{SUDP}, \text{NC}\}$. The state of the mobile client movement within a 2D space in an indoor environment can be modeled with a Markov chain $\Omega_{0:i} = \{\omega_0, \ldots, \omega_i\}$ which can be generated by $\omega_i \sim \mathcal{MC}(\pi^{(\omega)}, \overline{\mathbf{P}}^{(\omega)})$ with initial state PDF $\pi^{(\omega)} = \overline{p}\{\omega_0\}$. The initial state PDF, $\pi^{(\omega)}$, can then be related to the state probabilities and the average transition probabilities $\overline{\mathbf{P}}^{(\omega)} = \overline{p}_{i,j}^{(\omega)}$.

Following the methodology described in [27, 33], transition probabilities are defined as the rate of switching between Markov states or staying in the same state, accordingly, and they can be represented as

$$\overline{\mathbf{P}}^{(\omega)} = \begin{bmatrix} \overline{p}_{11}^{(\omega)} & \overline{p}_{12}^{(\omega)} & \overline{p}_{13}^{(\omega)} & \overline{p}_{14}^{(\omega)} \\ \overline{p}_{21}^{(\omega)} & \overline{p}_{22}^{(\omega)} & \overline{p}_{23}^{(\omega)} & \overline{p}_{24}^{(\omega)} \\ \overline{p}_{31}^{(\omega)} & \overline{p}_{32}^{(\omega)} & \overline{p}_{33}^{(\omega)} & \overline{p}_{34}^{(\omega)} \\ \overline{p}_{41}^{(\omega)} & \overline{p}_{42}^{(\omega)} & \overline{p}_{43}^{(\omega)} & \overline{p}_{44}^{(\omega)} \end{bmatrix}, \tag{10}$$

where $\overline{p}_{i,j}^{(\omega)}$ is defined as the average transition probability from the state i to the state j, as illustrated in Figure 3. These average transition probabilities can then be obtained using the following equation:

$$\overline{p}_{i,j}^{(\omega)} = \overline{p}(\omega_k = j \mid \omega_{k-1} = i). \tag{11}$$

From Figure 3, it can be concluded that transition from DDP state to NC state is only possible through one of the UDP states; so the resulting transition probabilities are set to zero, accordingly.

4.2. Average transition probabilities

Intuitively, the transition probability, that is, crossing rate between two states, is a function of the area of the states and the length of the boundary between the two states. Previous studies were mainly based on the statistics of such transitions. However, in this section, we present the details of obtaining the transition probabilities by discretizing the continuous problem, that is, forming a grid of receiver locations in the regions. Assuming that at time $t = t_k$ the mobile client is located at one of the grid points, then at $t = t_{k+1}$ the mobile client travels to one of the adjacent grid points. Let Δ represent grid size and let $T = t_{k+1} - t_k$ represent the sampling time. Thus $\Delta = v \times T$, where v represents the velocity of the mobile client. Furthermore, let α_c represent the crossing rate of the system which depends on the spatial pattern of movements. In our discrete model for indoor movements, assuming the walls are either horizontal or vertical, a mobile can only move in four directions. Assuming absolute randomness in the movement of the mobile client results in crossing rate probability of $\alpha_c = 1/4$ and staying in the same region with probability of $1 - \alpha_c$, as Figure 4 suggests. The average probability of crossing can then be obtained as

$$\overline{p}_{12} = \frac{\alpha_c \times (l/\Delta) + 0 \times (S_1/\Delta^2 - l/\Delta)}{S_1/\Delta^2}, \tag{12}$$

where l represents the boundary length of the two regions and S_1 represents the area of the first region. Simplifying (12) results in

$$\overline{p}_{12} = \alpha_c \times \frac{l \times \Delta}{S_1} = \alpha_c \times \frac{l \times vT}{S_1}. \tag{13}$$

Generalizing the results of the previous two states, that is, two-region random movement, to our Markov model with

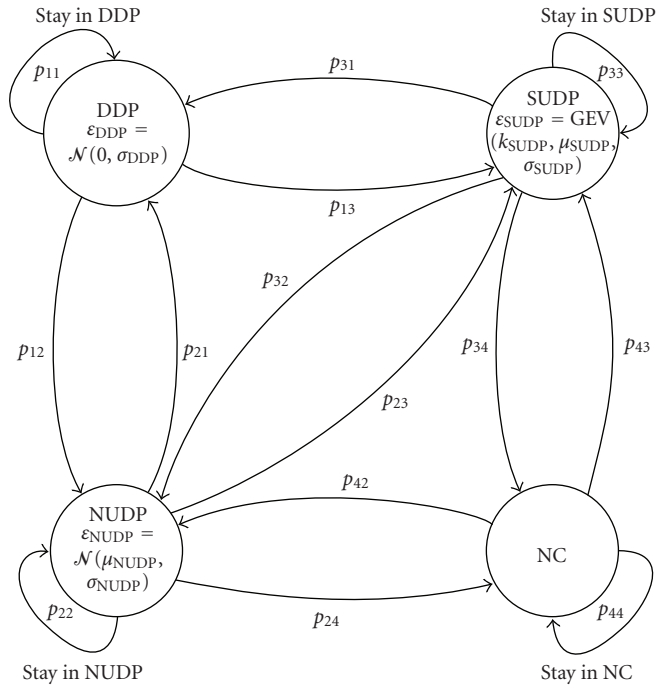

Figure 3: Markov model presented for dynamic behavior of the ranging error in indoor localization.

four states, we can obtain the transition probability matrix as

$$\overline{\mathbf{P}} = \begin{bmatrix} Q_1 & \alpha_c \frac{l_{12} \times vT}{S_1} & \alpha_c \frac{l_{13} \times vT}{S_1} & \alpha_c \frac{l_{14} \times vT}{S_1} \\ \alpha_c \frac{l_{21} \times vT}{S_2} & Q_2 & \alpha_c \frac{l_{23} \times vT}{S_2} & \alpha_c \frac{l_{24} \times vT}{S_2} \\ \alpha_c \frac{l_{31} \times vT}{S_3} & \alpha_c \frac{l_{32} \times vT}{S_3} & Q_3 & \alpha_c \frac{l_{34} \times vT}{S_3} \\ \alpha_c \frac{l_{41} \times vT}{S_4} & \alpha_c \frac{l_{42} \times vT}{S_4} & \alpha_c \frac{l_{43} \times vT}{S_4} & Q_4 \end{bmatrix}, \tag{14}$$

where Q_1 denotes $1 - \alpha_c((l_{12} + l_{13} + l_{14}) \times vT/S_1)$, Q_2 denotes $1 - \alpha_c((l_{21} + l_{23} + l_{24}) \times vT/S_2)$, Q_3 denotes $1 - \alpha_c((l_{31} + l_{32} + l_{34}) \times vT/S_3)$, Q_4 denotes $1 - \alpha_c((l_{41} + l_{42} + l_{43}) \times vT/S_4)$, and $l_{ij} = l_{ji}$ represents the boundary length between ith and jth regions and S_k represents the area of the kth region. Combining α_c and vT parameters, we can obtain

$$\overline{\mathbf{P}} = \begin{bmatrix} W_1 & \beta \frac{l_{12}}{S_1} & \beta \frac{l_{13}}{S_1} & \beta \frac{l_{14}}{S_1} \\ \beta \frac{l_{12}}{S_2} & W_2 & \beta \frac{l_{23}}{S_2} & \beta \frac{l_{24}}{S_2} \\ \beta \frac{l_{13}}{S_3} & \beta \frac{l_{23}}{S_3} & W_3 & \beta \frac{l_{34}}{S_3} \\ \beta \frac{l_{14}}{S_4} & \beta \frac{l_{24}}{S_4} & \beta \frac{l_{34}}{S_4} & W_4 \end{bmatrix}, \tag{15}$$

where W_1 denotes $1 - \beta((l_{12} + l_{13} + l_{14})/S_1)$, W_2 denotes $1 - \beta((l_{12} + l_{23} + l_{24})/S_2)$, W_3 denotes $1 - \beta((l_{13} + l_{23} + l_{34})/S_3)$, W_4 denotes $1 - \beta((l_{14} + l_{24} + l_{34})/S_4)$, and $\beta = \alpha_c \times vT$ represents both the velocity of the mobile client and the probability of crossing among the regions as well as the sole parameter to be determined. In the case of indoor positioning, the DDP and NC regions are not connected directly, resulting in $l_{14} = l_{41} = 0$, which confirms the absence of the link between DDP and NC states in Figure 3.

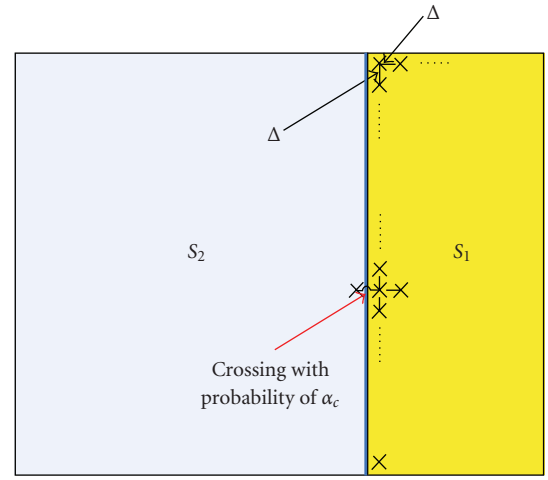

Figure 4: Crossing rate of a random mobile client from one Markov state to another.

4.3. Exponential modeling of average staying time

As discussed in [33], the Markov property reveals the following in regard to the eigenvectors of $\overline{\mathbf{P}}$:

$$\varphi_1 = 1, \quad |\varphi_i| < 1 \Longrightarrow \overline{\mathbf{P}} v_i = \varphi_i v_i, \tag{16}$$

where φ_i represents the eigenvalues of $\overline{\mathbf{P}}$ and v_i represents the eigenvectors associated with φ_i. For the presented Markov model, $v_i = [e_1 \ e_2 \ e_3 \ e_4]$ and $\sum e_i = 1$, representing the normalized eigenvector. We concentrate on the steady state probabilities as the Markov chain settles into stationary behavior after the process has been running for a long time. When this occurs, we have

$$\overline{\mathbf{P}} v_1 = v_1 \tag{17}$$

which represents the eigenvector associated with $\varphi_1 = 1$ and determines the expected average waiting time in each state. Next, assuming homogeneous transition probabilities in continuous time, that is, $P[X(s+t) = j \mid X(s) = i] = P[X(t) = j \mid X(0) = i] = p_{ij}(T_n)$, we convert the discrete Markov chain in (15) to an equivalent continuous-time Markov chain to extract the staying time distributions of each state. The memoryless distribution of the staying time in a certain state can then only be described by an exponential random variable $p[\mathrm{T} > t] = e^{-\gamma_i t}$ [33]. Similar to the methodology described in [33], γ_is can be determined by solving the respective Chapman-Kolmogorov equation and equating γ_i to $-1/\theta_{ii}$, with θ being the solution of Chapman-Kolmogorov equation. The solution for the Chapman-Kolmogorov equation for the steady state $\overline{\mathbf{P}}$ results in

$$\theta = \begin{bmatrix} R_1 & \beta \times \frac{l_{12}}{S_1} & \beta \times \frac{l_{13}}{S_1} & \beta \times \frac{l_{14}}{S_1} \\ \beta \times \frac{l_{12}}{S_2} & R_2 & \beta \times \frac{l_{23}}{S_2} & \beta \times \frac{l_{24}}{S_2} \\ \beta \times \frac{l_{13}}{S_3} & \beta \times \frac{l_{23}}{S_3} & R_3 & \beta \times \frac{l_{34}}{S_3} \\ \beta \times \frac{l_{14}}{S_4} & \beta \times \frac{l_{24}}{S_4} & \beta \times \frac{l_{34}}{S_4} & R_4 \end{bmatrix}, \tag{18}$$

where R_1 denotes $-\beta \times (l_{12} + l_{13} + l_{14})/S_1$, R_2 denotes $-\beta \times (l_{12} + l_{23} + l_{24})/S_2$, R_3 denotes $-\beta \times (l_{13} + l_{23} + l_{34})/S_3$, and R_4 denotes $-\beta \times (l_{14} + l_{24} + l_{34})/S_4$, which in the case of the presented Markov model leads to

$$[\gamma_1 \ \ \gamma_2 \ \ \gamma_3 \ \ \gamma_4] = [B_1 \ \ B_2 \ \ B_3 \ \ B_4], \tag{19}$$

where B_1 denotes $S_1/\beta(l_{12}+l_{13}+l_{14})$, B_2 denotes $S_2/\beta(l_{12}+l_{23}+l_{24})$, B_3 denotes $S_3/\beta(l_{13}+l_{23}+l_{34})$, and B_4 denotes $S_4/\beta(l_{14}+l_{24}+l_{34})$.

Determining exponential parameters allows us to simulate the average waiting time in each state and compare them with the results of the empirical data.

4.4. Multivariate distribution modeling of the state probabilities

Intuitively, altering the location of the transmitter will change the state probabilities; for example, a transmitter location close to the obstructive metallic object will cause larger set of SUDP receiver locations. The histogram of the state probabilities can then be modeled by a multivariate distribution, as the state probabilities are not clearly independent. In order to find the best distribution to model the state probabilities, we altered the location of the transmitter in the floor plan of the building under study and investigated the histograms and probability plots of the state probabilities. As it is shown in the following section, a practical choice for the multivariate distribution is Gaussian distribution which leads us to form a joint Gaussian distribution to model the state probabilities of the main three states. The fourth state can then be found deterministically as the sum of the state probabilities should be equal to unity. Therefore, we can start with a multivariate normal distribution to represent the state probabilities:

$$f_{\mathbf{Y}}(\mathbf{y}) = (2\pi)^{-3/2} |\boldsymbol{\Sigma}|^{-1/2} \exp\left(-\frac{1}{2} (\mathbf{y} - \overline{\boldsymbol{\mu}})^T \boldsymbol{\Sigma}^{-1} (\mathbf{y} - \overline{\boldsymbol{\mu}}) \right), \tag{20}$$

where $\mathbf{y} = \left[\overline{P}_{\mathrm{DDP}} \ \ \overline{P}_{\mathrm{NUDP}} \ \ \overline{P}_{\mathrm{SUDP}}\right]$ represents the random vector containing the average state probability values, $\boldsymbol{\Sigma}$ and $\overline{\boldsymbol{\mu}}$ are the parameters of the joint distribution, and T represents the transpose of a vector. In order to extract the parameters of this multivariate normal distribution, we used sample mean to approximate the mean as

$$\hat{\overline{\boldsymbol{\mu}}} = \frac{1}{n} \sum_{k=1}^{n} P_{z_k}, \quad z \in \{\mathrm{DDP}, \mathrm{NUDP}, \mathrm{SUDP}\}, \tag{21}$$

where P_{z_k} represents the kth observed state probability of the state z, and n represents the total number of observations. The maximum likelihood estimator of the covariance matrix can then be defined as

$$\hat{\boldsymbol{\Sigma}} = \left(\frac{1}{n-1}\right) \sum_{k=1}^{n} \left(\mathbf{P}_{\mathbf{z_k}} - \hat{\overline{\boldsymbol{\mu}}}\right) \left(\mathbf{P}_{\mathbf{z_k}} - \hat{\overline{\boldsymbol{\mu}}}\right)^T, \tag{22}$$

where $\hat{\overline{\boldsymbol{\mu}}}$ is the sample mean, $\mathbf{P}_{\mathbf{z_k}} = \left[P_{\mathrm{DDP}_k} \ \ P_{\mathrm{NUDP}_k} \ \ P_{\mathrm{SUDP}_k}\right]$ represents the kth state probability observation, and n represents the total number of observations.

Now with the aid of Cholesky decomposition, we provide a method for reconstructing the state probabilities in a typical indoor scenario. In communication realm, Cholesky decomposition is used in synchronization and noise suppression [34, 35]. Similar to [36], in order to regenerate these state probabilities, one may pursue the following procedure. The first step is to decompose the covariance matrix using Cholesky decomposition method:

$$AA^T = \hat{\boldsymbol{\Sigma}}, \tag{23}$$

then we generate a vector of standard normal values $\mathbf{Z}$, and use the following equation:

$$\breve{\mathbf{y}} = \hat{\overline{\boldsymbol{\mu}}} + A\mathbf{Z}, \tag{24}$$

where $\breve{\mathbf{y}} = [P_{\mathrm{DDP}} \ P_{\mathrm{NUDP}} \ P_{\mathrm{SUDP}}]$ represents the generated values of state probabilities.

We refer to this method of extracting state probabilities as multivariate normal distribution (MND) model throughout this paper.

5. SIMULATION AND RESULTS

To completely model the dynamic behavior of ranging error observed in indoor environment, the transition probabilities of the Markov chain and statistics of ranging error for each Markov state are required. Thus, we started the process by categorizing the receiver locations according to (7). Once the class of each receiver location and consequently the Markov state associated with it were identified, different distributions for statistics of ranging error observed in each class are introduced and modeled. Consequently, by collecting the area of each state and the boundary length between each two states, the transition probabilities were acquired based on (15). Finally, we modeled the dynamic behavior of the ranging error by running the Markov chain, and we compared the results of analytical derivation obtained from Section 4 to RT simulation of a dynamic scenario observed in the sample indoor environment. Furthermore, altering the location of the transmitter and gathering the observed values for state probabilities of each state enabled us to model the statistics of state probabilities and initialize the Markov chain.

For the purpose of the simulation, we considered the third floor of AK Labs at WPI as the floor plan of the building under study which resembles typical indoor office environment; yet it is a really harsh environment due to the existence of extensive blocks of metallic objects in the building. We formed a grid of receiver locations in the floor plan, approximately 14000 receiver locations, and generated their respective CIRs for different locations of the transmitter. In order to simulate the real-time channel profile of the CIR, a finite bandwidth raised-cosine filter can be used to extract the channel profile. For the purpose of ToA-based localization, it is shown that a minimum bandwidth of 200 MHz is sufficient for effectively resolving the multipath components and combating the multipath-induced error [4]. However, we used a 5 GHz raised-cosine filter to obtain a more realistic channel profile captured by an UWB measurement system. Postprocessing peak detection algorithm is then used to estimate τ_{FDP} and consequently form the error, as discussed in Section 2.

5.1. Ranging error modeling for different classes of receiver locations

Modeling the ranging error observed in different classes of receiver locations in indoor localization is the major challenge in the analysis of an indoor positioning system. It is a common belief that occurring ranging errors associated with LoS state (and equivalently DDP state) can be simulated with Gaussian distribution [18]. However, in NLoS conditions, and equivalently in NUDP and SUDP states, different distributions consisting of Gaussian [18], exponential [14, 22], log-normal [37, 38], and mixture of exponential and Gaussian [19, 39] have been used for modeling the ranging error. Comprehensive UWB measurement and modeling of ranging errors in NLoS can be found in [40] which reports a heavy-tail distribution for ranging errors observed in UDP conditions. In this section, we provide precise distribution for modeling the ranging error associated with each state.

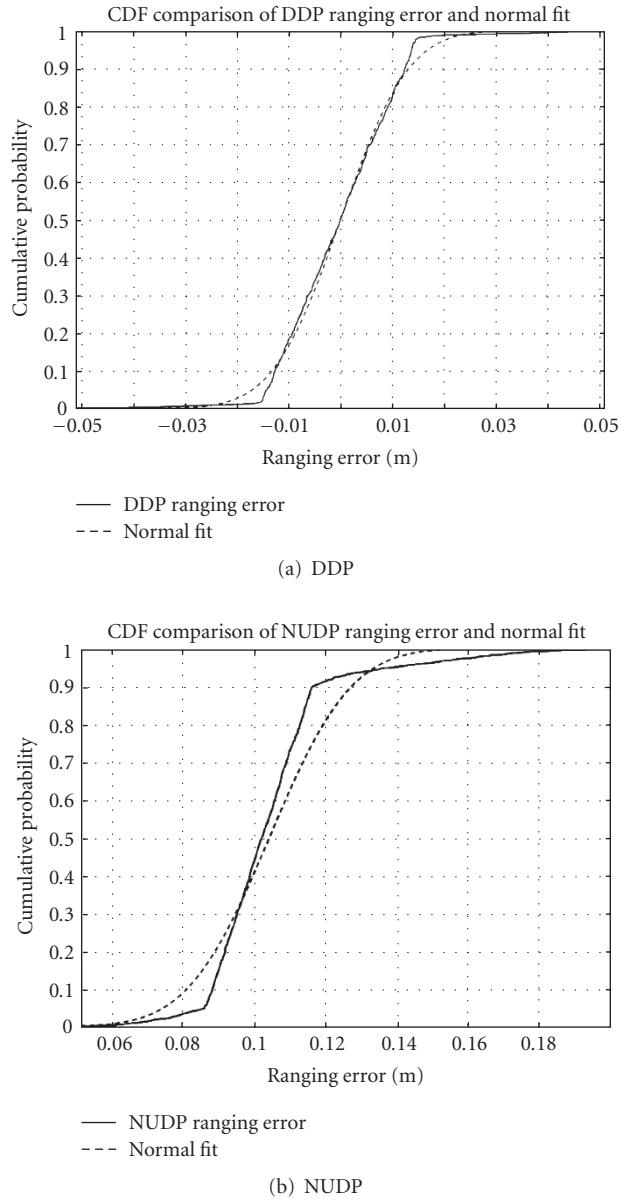

Figure 5: Distribution modeling of the ranging error with normal distribution for (a) DDP class of receiver locations and (b) NUDP class of receiver locations.

For each class of receiver locations, we provide the histogram and, if necessary, the probability plot of the error for visualization of the goodness of fit.

Figure 5(a) compares the CDF of the observed ranging error for DDP class of receiver locations with its respective normal distribution fit. In DDP class of receiver locations, $\lambda_i = 0$, and using (4) leads us to

$$f_{\varepsilon_{\mathrm{DDP}}}(\varepsilon) = f^{\mathbf{M}}(\varepsilon) = \mathcal{N}(\mu_{\mathrm{DDP}}, \sigma_{\mathrm{DDP}}). \tag{25}$$

Similarly, Figure 5(b) compares the CDF of NUDP ranging error with its normal distribution fit. It can be noticed that although the CDF of ranging errors is similar in case of DDP and NUDP ranging errors, the NUDP ranging errors

Table 1: Parameters of normal distribution and ranging error of DDP and NUDP classes.

	Normal distribution	
DDP ranging error	μ_{DDP}	σ_{DDP}
	0.0135	0.0105
NUDP ranging error	μ_{NUDP}	σ_{NUDP}
	0.1063	0.0239

Table 2: Passing rate of $K-S$ and statistical value of χ^2 hypothesis tests at 5% significance level, and ranging error for SUDP class.

Distribution	SUDP		
	$K-S$	χ^2	*Akaike weight*
Normal	78.71%	50.84%	0
Weibull	85.02%	74.91%	8.6×10^{-10}
GEV	96.86%	85.31%	1
Log-normal	87.82%	67.11%	6.4×10^{-17}

tend to be more positive. Therefore, the distribution of ranging error can be represented as

$$f_{\varepsilon_{\text{NUDP}}}(\varepsilon) = f^{\mathbf{M+NUDP}}(\varepsilon) = \mathcal{N}(\mu_{\text{NUDP}}, \sigma_{\text{NUDP}}), \tag{26}$$

where $\mu_{\text{NUDP}} > \mu_{\text{DDP}}$.

Our explanation to such observation is the presence of propagation delay and the larger separation of the antenna pair, which allow multipath and loss of the DP to be more effective. Table 1 provides the statistics of ranging errors observed in such classes of receiver locations.

In SUDP class of receiver locations, the ranging errors are following a heavy-tail distribution which cannot be modeled with a Gaussian distribution. It can be observed that in such scenarios, the infrastructure of the indoor environment commonly obstructs the DP component and causes unexpected larger ranging errors. As a result, the statistical characteristics of the ranging error in SUDP class exhibit a heavy-tail phenomenon in its distribution function. This heavy-tail phenomenon has been reported and modeled in the literature. As in [19, 39], the observed ranging error was modeled as a combination of a Gaussian distribution and an exponential distribution, and the work in [37, 38] modeled the ranging error with a log-normal distribution.

Traditionally, log-normal, Weibull, and generalized extreme value (GEV) distributions are used to model the phenomenon with heavy tail. The GEV class of distributions, with three degrees of freedom, is applied to model the extreme events in hydrology, climatology, and finance [41].

Table 2 summarizes the results of the $K-S$ test and χ^2 test for SUDP class of different distributions. It can be observed that from the distributions offered to model the SUDP ranging error, normal distribution fails both $K-S$ and χ^2 hypothesis tests, while the rest of distributions pass the hypothesis tests.

Figure 6(a) compares the PDF of the ranging error for SUDP state with its respective normal, Weibull, GEV, and log-normal fits. Figure 6(b) illustrates the probability plot and the closeness of the fits for SUDP class. From Table 2, it can be also observed that GEV distribution passing rate is the highest amongst all distributions, which is expected as GEV models the heavy-tail phenomenon with three degrees of freedom compared to two degrees of freedom of log-normal and Weibull distributions. Similar observations have been reported in [40] using UWB measurements conducted in different indoor environments. Quantitatively, for the selection of the best distribution, we refer to the Akaike information criterion [42], represented in Table 2, by forming the log-likelihood function of the candidate distribution and penalizing each distribution with its respective number of parameters to be estimated. Following the methodology described in [42], the Akaike weights can be used to determine the best model which fits the empirical data. The higher values of Akaike weight represent more plausible distribution, and the highest value can be associated with the best model. The result of such experiment also confirms the result of probability plot and suggests that the best distribution to model the ranging error associated with SUDP class is in fact a GEV distribution, since all the other Akaike weights are practically zero.

Table 3: Parameters of GEV distribution and ranging error of SUDP class.

	GEV distribution		
SUDP ranging error	μ_{SUDP}	σ_{SUDP}	k_{SUDP}
	2.5218	1.2844	0.4198

The GEV distribution is defined as

$$f(x \mid k, \mu, \sigma) = \left(\frac{1}{\sigma}\right)\exp\left(-\left(1+k\frac{(x-\mu)}{\sigma}\right)^{-1/k}\right)\left(1+k\frac{(x-\mu)}{\sigma}\right)^{-1-1/k}, \tag{27}$$

for $1+k((x-\mu)/\sigma) > 0$, where μ is defined as the location parameter, σ is defined as the scale parameter, and k is the shape parameter. The value of k defines the type of the GEV distribution; $k = 0$ is associated with type I, also known as Gumbel, and $k < 0$ is associated with type II, which is also correspondent to Weibull. However, type III, associated with $k > 0$, which is known as Frechet type, best models the heavy tail observed in ranging errors associated with SUDP class of receiver locations. Parameters of the GEV distribution, modeling the ranging error observed in SUDP class of receiver locations, are reported in Table 3. Evidentally, it can be noted that the presented GEV distribution for ranging errors observed in SUDP class of receiver locations belongs to the third category with its respective $k > 0$. Hence,

$$f_{\varepsilon_{\text{SUDP}}}(\varepsilon) = f^{\mathbf{M+NUDP+SUDP}}(\varepsilon) = \mathcal{GEV}(\mu_{\text{SUDP}}, \sigma_{\text{SUDP}}, k_{\text{SUDP}}), \tag{28}$$

where $k_{\text{SUDP}} > 0$.

Next we relate the statistics of the ranging errors observed in different classes of receiver locations to the parameters of the cluster model defined in IEEE 802.15.3 (see (2). It is important to notice that the small ranging error values reported

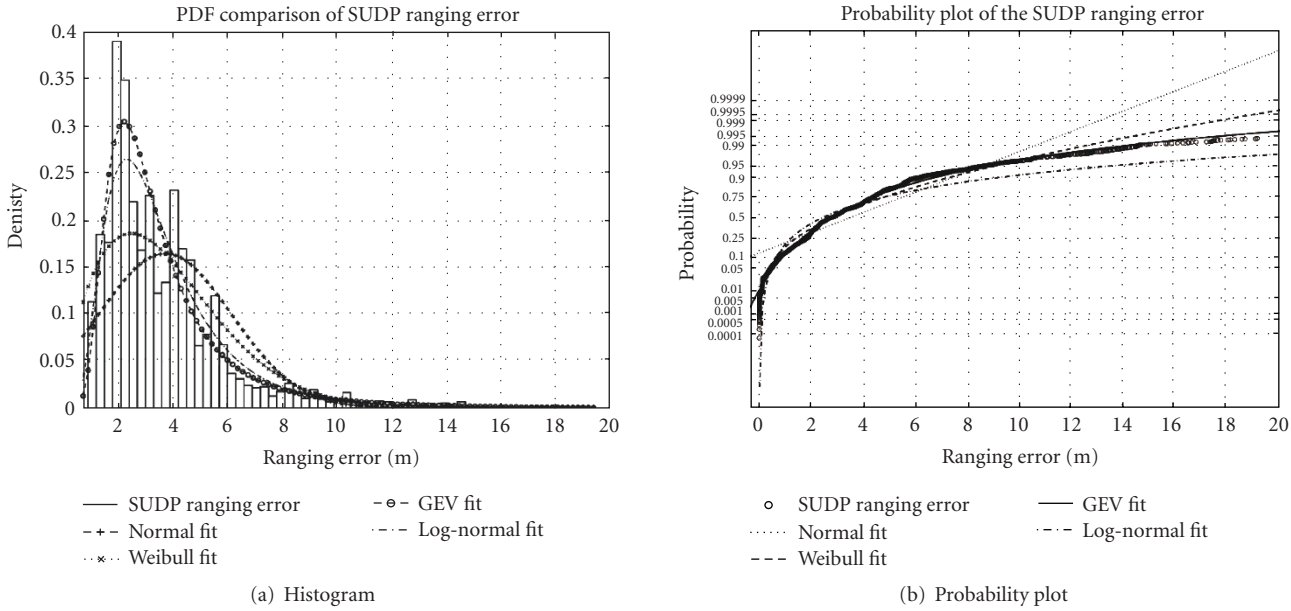

(a) Histogram (b) Probability plot

Figure 6: Statistical analysis of ranging error observed in SUDP class of receiver locations. (a) Histogram of ranging error and (b) probability plot of ranging error versus different distributions. It can be concluded that GEV distribution best models the ranging error observed in such class of receiver locations.

for DDP and NUDP classes enable the user to use the channel models reported in IEEE *P*802.15.3 [10, 12, 15] for ranging purposes, while larger ranging errors observed in SUDP region prevent such model from being used for ranging purposes.

5.2. Improvement over IEEE 802.15.3 recommended model

IEEE 802.15.3 is assumed, through (2), to be the basic discrete model of the wireless channel in indoor environment. From our observations, in DDP class, since the DP is easily detected, ranging error is at its minimum. Although it is shown that DDP state multipath error exists [18], for UWB systems the multipath error is in the order of few centimeters, which is acceptable for cooperative localization and wireless sensor networks. In NUDP class, we hypothesize that the first cluster is detected. However, the power of DP is not within the dynamic range of the receiver, which results in detecting the second path (or any of the following paths after DP) as the FDP. Therefore, the error should be approximated with the ray arrival rate in the IEEE 802.15.3 model. It is reported that the ray arrival rate is in the order of $\lambda = 2.1(1/\text{nsec})$. By detecting the following paths with the specified arrival rate, an error of $(1/\lambda \times 10^{-9} \times c = 0.15)$ meters is expected, which is in agreement with the average error observed in the NUDP state and reported in Table 1.

However, in the SUDP class, which is characterized by extreme NLoS condition in IEEE 802.15.3, blockage of the first cluster results in detecting a path from the next cluster, and hence the receiver makes an unexpectedly large error. IEEE *P*802.15.3 model provides the cluster arrival rate of $\Lambda = 0.0667(1/\text{nsec})$; hence algorithm makes a ranging error in the order of $(1/\Lambda \times 10^{-9} \times c = 4.5)$ meters. The mean of the GEV distribution is given by $\mu - \sigma/k + \sigma/k \times \Gamma(1-k)$, where $\Gamma(x)$ represents the gamma function. Substituting the reported parameters of SUDP ranging error yields an average of 4.31 meters, which on average is in agreement with the assumption of loss of the first cluster. Based on this analysis, we recommend that if IEEE 802.15.3 model is being used for ToA-based ranging purposes in extreme NLoS conditions, slight modifications are necessary for acquiring tangible estimate of the ranging error observed in such conditions.

5.3. Markov model representation

The transition probabilities in Markov chain are analytically obtained using IDM realization, capturing the areas and boundary lengths and consequently using (15). To validate the analytical derivation of transition probabilities of Markov chain, we consider a *random walk* process traveled by the mobile user in the third floor scenario of the AK Labs at WPI, as shown in Figure 1. In this *random walk* process, we calculate the number of state transitions and compare them to the analytical derivation in (15).

5.3.1. Parameters of the Markov chain

The generated 14000 CIRs for the different receiver locations in the building were categorized into DDP, NUDP, SUDP, and NC classes using (7). The *random walk* was designed in a way to simulate a random mobile client traveling in indoor environment. It is assumed that the mobile client travels on the vertical or horizontal routes and continues its route until next node, that is, door or hallway, and then it randomly chooses the next node and travels towards it. This type of

movement results in crossing the borders of states whenever mobile client is close to the boundary of two states, yielding $\alpha_c \simeq 1$. The separation of the movement at each time instant, that is, 1 second, is 14.28 cm, resulting in $vT \simeq 1/7$. Furthermore, according to the IDM model, the parameters of the floor plan are

$$\begin{aligned} l_{12} &= 17.07\,(\text{m}), & l_{13} &= 28.48\,(\text{m}),\\ l_{14} &= 0\,(\text{m}), & S_1 &= 255.02\,(\text{m}^2),\\ l_{21} &= 17.07\,(\text{m}), & l_{23} &= 23.34\,(\text{m}),\\ l_{24} &= 14.00\,(\text{m}), & S_2 &= 217.51\,(\text{m}^2),\\ l_{31} &= 28.48\,(\text{m}), & l_{32} &= 23.34\,(\text{m}),\\ l_{34} &= 16.70\,(\text{m}), & S_3 &= 164.03\,(\text{m}^2),\\ l_{41} &= 0\,(\text{m}), & l_{42} &= 14.00\,(\text{m}),\\ l_{43} &= 16.70\,(\text{m}), & S_4 &= 299.60\,(\text{m}^2), \end{aligned} \tag{29}$$

which according to the analytical derivation of Section 4 forms a transition probability matrix of

$$\mathbf{P} = \begin{bmatrix} 0.9744 & 0.0095 & 0.0159 & 0 \\ 0.0112 & 0.9642 & 0.0153 & 0.0091 \\ 0.0248 & 0.0203 & 0.9403 & 0.0145 \\ 0 & 0.0066 & 0.0079 & 0.9853 \end{bmatrix}. \tag{30}$$

On the other hand, once the class of each receiver location was identified, we generated 7000 CIRs associated with the receiver locations of the *random walk* to empirically calculate the transition probability matrix of the Markov model. We repeated the steps for several different configurations of *random walk* inside the building under study and averaged the transition probabilities. The experiment yielded

$$\mathbf{P} = \begin{bmatrix} 0.9645 & 0.0085 & 0.027 & 0 \\ 0.0126 & 0.9501 & 0.0156 & 0.0217 \\ 0.0259 & 0.0179 & 0.9322 & 0.024 \\ 0 & 0.0108 & 0.0169 & 0.9723 \end{bmatrix}, \tag{31}$$

which, considering the fact that the type of movement implies $\beta = \alpha \times vT \simeq 1/7$, is very close to the analytical transition probability obtained from (15) and reported in (30). The differences between the two matrices are mainly due to the pattern of *random walk,* as it only considers moving along hallways and in and out of offices. Note that $\overline{p}_{14} = \overline{p}_{41} = 0$ in both matrices confirms the absence of the link between DDP and NC classes. It is worth mentioning that altering the parameters of the simulation such as η, α, and v results in different transition probabilities.

For our second measure of validity of the Markov model, we used state occupancy times. Finding the vector associated with the exponential parameters of **P**, we can compare CDFs of the width of staying times of different classes of receiver locations. The corresponding waiting time vector is found to be

$$v = [39.19 \quad 27.98 \quad 16.75 \quad 68.31], \tag{32}$$

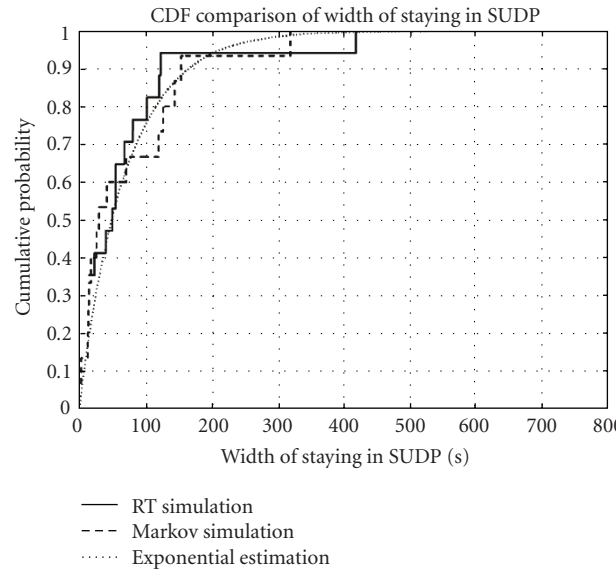

Figure 7: Comparison of width of staying in SUDP state for simulation and modeling.

which yields the parameters of the exponential model of residing in each state for DDP, NUDP, SUDP, and NC states, respectively.

We simulated the exponential distributions and compared them to the width of the staying times resulting from RT simulation and width of staying times obtained from running the Markov chain. Figure 7 represents the CDF comparison of width of staying times in SUDP class of receiver locations. It is worth mentioning that other Markov states demonstrate similar close fits.

5.3.2. Ranging error statistics

As discussed in Section 4.2, empirical models using measurement and RT have confirmed that ranging errors occurring in DDP and NUDP states can be modeled with normal distribution whose moments are functions of the bandwidth of the channel [18, 27]. However, in SUDP class of receiver locations, the distribution which fits the observed ranging error is GEV. Tables 1 and 3 summarize the statistics of ranging error for different states of the presented Markov model for a bandwidth of 5 GHz obtained from the analysis of CIRs of the same 14000 receiver locations on the third floor of the AK Labs.

Using the statistics of ranging error and the parameters of the Markov model of Figure 3 provided by (15) enables us to simulate the dynamic behavior of ranging error observed by the mobile user. In order to validate the effectiveness of the Markov model, we initialized the Markov model with an estimate of state probabilities obtained from MND model, and ran the Markov process with the transition probabilities reported in (30). According to the class of ranging errors produced by Markov model, we simulated the ranging error of each state by using parameters of Tables 1 and 3. Figure 8 compares the CDF of total ranging error observed

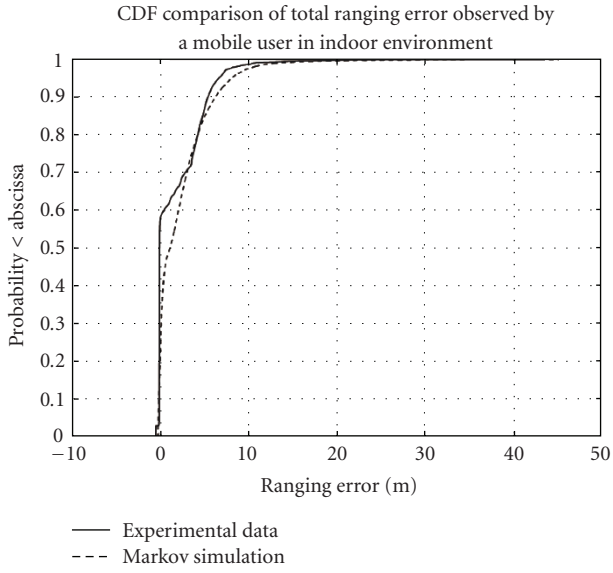

Figure 8: Comparison of ranging error observed by a mobile user with simulation.

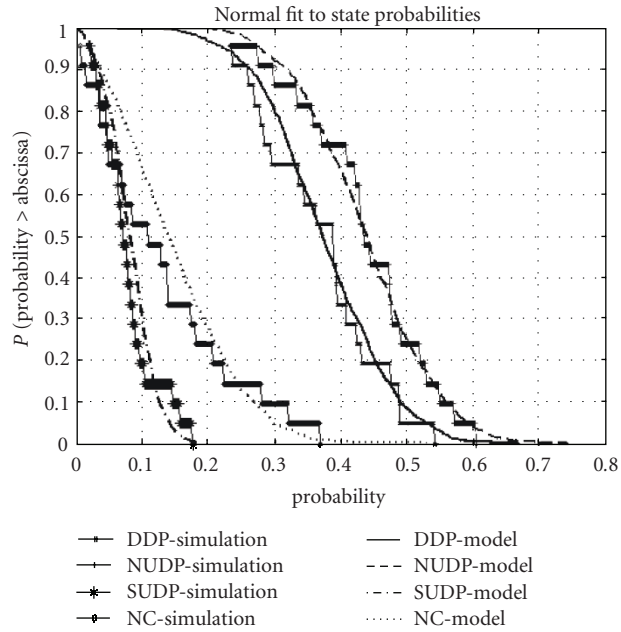

Figure 9: Comparison of the CDF of the state probabilities for different states with their respective normal fit.

by the mobile user traveling in indoor environment for empirical data using simulation and analytical dynamic Markov model. It is worth mentioning that comparisons of empirical and simulated ranging errors observed in individual classes also show close agreement.

5.4. Modeling and analysis of state probabilities

For the building under study, varying the location of the transmitter and recording the state probabilities using IDM realization yielded

$$\hat{\vec{\mu}} = [0.3662 \quad 0.4332 \quad 0.0747],$$
$$\hat{\Sigma} = \begin{bmatrix} 0.0081 & -0.0015 & 0.004 \\ -0.0015 & 0.0096 & -0.0031 \\ 0.004 & -0.0031 & 0.0018 \end{bmatrix}. \tag{33}$$

Following the Cholesky decomposition method and regenerating the state probabilities, we can approximate the parameters of the MND model and compare the MND model with the result of simulation. Figure 9 illustrates the reconstruction of the state probabilities with 100 iterations for the main three states using MND model. The NC state can be found deterministically using

$$P_{\mathrm{NC}} = 1 - P_{\mathrm{DDP}} - P_{\mathrm{NUDP}} - P_{\mathrm{SUDP}}. \tag{34}$$

It can be observed that the MND model-generated state probabilities closely follow IDM.

6. CONCLUSION

In this paper, we presented a novel application of Markov chain for modeling the dynamic behavior of the ranging error in a typical indoor localization application which assists us in the design and performance evaluation of tracking capabilities of such systems. The parameters of the Markov model and exponential waiting times were obtained from analytical derivation based on real UWB measurement conducted on the third floor of the AK Labs. The parameters of distributions of ranging error observed in each Markov state were extracted from empirical data obtained from 14000 channel impulse responses on the third floor of the AK Labs at WPI. The results of simulation for the dynamic behavior of ranging error using the Markov chain were shown to provide close agreement with the results of empirical data.

ACKNOWLEDGMENTS

The material presented in this paper was partially prepared during a joint project collaboration between Charles Stark Draper Laboratory and CWINS at WPI. The authors would like to thank Dr. Allen Levesque and Nayef A. Alsindi at WPI for their constructive review and comments.

REFERENCES

[1] K. Pahlavan, X. Li, and J.-P. Mäkelä, "Indoor geolocation science and technology," *IEEE Communications Magazine*, vol. 40, no. 2, pp. 112–118, 2002.

[2] A. H. Sayed, A. Tarighat, and N. Khajehnouri, "Network-based wireless location: challenges faced in developing techniques for accurate wireless location information," *IEEE Signal Processing Magazine*, vol. 22, no. 4, pp. 24–40, 2005.

[3] K. Pahlavan, P. Krishnamurthy, and J. Beneat, "Wideband radio propagation modeling for indoor geolocation applications," *IEEE Communications Magazine*, vol. 36, no. 4, pp. 60–65, 1998.

[4] K. Pahlavan, F. O. Akgül, M. Heidari, A. Hatami, J. M. Elwell, and R. D. Tingley, "Indoor geolocation in the absence of direct path," *IEEE Wireless Communications*, vol. 13, no. 6, pp. 50–58, 2006.

[5] A. Saleh and R. Valenzuela, "A statistical model for indoor multipath propagation," *IEEE Journal on Selected Areas in Communications*, vol. 5, no. 2, pp. 128–137, 1987.

[6] T. S. Rappaport, S. Y. Seidel, and K. Takamizawa, "Statistical channel impulse response models for factory and open plan building radio communication system design," *IEEE Transactions on Communications*, vol. 39, no. 5, pp. 794–807, 1991.

[7] H. Hashemi, "The indoor radio propagation channel," *Proceedings of the IEEE*, vol. 81, no. 7, pp. 943–968, 1993.

[8] H. Hashemi, "Impulse response modeling of indoor radio propagation channels," *IEEE Journal on Selected Areas in Communications*, vol. 11, no. 7, pp. 967–978, 1993.

[9] B. Alavi, *Distance measurement error modeling for time-of-arrival based indoor geolocation*, Ph.D. thesis, Worcester Polytechnic Institute, Worcester, Mass, USA, 2006.

[10] A. F. Molisch, J. R. Foerster, and M. Pendergrass, "Channel models for ultrawideband personal area networks," *IEEE Wireless Communications*, vol. 10, no. 6, pp. 14–21, 2003.

[11] A. F. Molisch, D. Cassioli, C.-C Chong, et al., "A comprehensive standardized model for ultrawideband propagation channels," *IEEE Transactions on Antennas and Propagation*, vol. 54, no. 11, pp. 3151–3166, 2006.

[12] D. Cassioli, M. Z. Win, and A. F. Molisch, "The ultra-wide bandwidth indoor channel: from statistical model to simulations," *IEEE Journal on Selected Areas in Communications*, vol. 20, no. 6, pp. 1247–1257, 2002.

[13] S. S. Ghassemzadeh, R. Jana, C. W. Rice, W. Turin, and V. Tarokh, "Measurement and modeling of an ultra-wide bandwidth indoor channel," *IEEE Transactions on Communications*, vol. 52, no. 10, pp. 1786–1796, 2004.

[14] S. S. Ghassemzadeh, L. J. Greenstein, T. Sveinsson, A. Kavcic, and V. Tarokh, "UWB delay profile models for residential and commercial indoor environments," *IEEE Transactions on Vehicular Technology*, vol. 54, no. 4, pp. 1235–1244, 2005.

[15] A. F. Molisch, "Ultrawideband propagation channels-theory, measurement, and modeling," *IEEE Transactions on Vehicular Technology*, vol. 54, no. 5, pp. 1528–1545, 2005.

[16] C. Falsi, D. Dardari, L. Mucchi, and M. Z. Win, "Time of arrival estimation for UWB localizers in realistic environments," *EURASIP Journal on Applied Signal Processing*, vol. 2006, Article ID 32082, 13 pages, 2006.

[17] S. Gezici, Z. Tian, G. B. Giannakis, et al., "Localization via ultra-wideband radios: a look at positioning aspects of future sensor networks," *IEEE Signal Processing Magazine*, vol. 22, no. 4, pp. 70–84, 2005.

[18] B. Alavi and K. Pahlavan, "Modeling of the TOA-based distance measurement error using UWB indoor radio measurements," *IEEE Communication Letter*, vol. 10, no. 4, pp. 275–277, 2006.

[19] B. Denis and N. Daniele, "NLOS ranging error mitigation in a distributed positioning algorithm for indoor UWB Ad-hoc Networks," in *IEEE International Workshop on Wireless Ad-Hoc Networks (IWWAN '05)*, pp. 356–360, London, UK, May-June 2005.

[20] J. L. Krolik and R. H. Anderson, "Maximum likelihood coordinate registration for over-the-horizon radar," *IEEE Transactions on Signal Processing*, vol. 45, no. 4, pp. 945–959, 1997.

[21] A. M. Ladd, K. E. Berkis, A. P. Rudys, D. S. Wallach, and L. E. Kavraki, "On the feasability of using wireless ethernet for indoor localization," *IEEE Transactions on Robotics and Automation*, vol. 20, no. 3, pp. 555–559, 2004.

[22] C. Morelli, M. Nicoli, V. Rampa, and U. Spagnolini, "Hidden Markov models for radio localization in mixed LOS/NLOS conditions," *IEEE Transactions on Signal Processing*, vol. 55, no. 4, pp. 1525–1542, 2007.

[23] G. Yang, K. Pahlavan, and T. J. Holt, "Sector antenna and DFE modems for high speed indoor radio communications," *IEEE Transactions on Vehicular Technology*, vol. 43, no. 4, pp. 925–933, 1994.

[24] A. Falsafi, K. Pahlavan, and G. Yang, "Transmission techniques for radio LAN's—a comparative performance evaluation using ray tracing," *IEEE Journal on Selected Areas in Communications*, vol. 14, no. 3, pp. 477–491, 1996.

[25] K. Pahlavan and A. H. Levesque, *Wireless Information Networks*, John Wiley & Sons, New York, NY, USA, 2nd edition, 2005.

[26] M. Heidari and K. Pahlavan, "A new statistical model for the behavior of ranging errors in TOA-based indoor localization," in *IEEE Wireless Communications and Networking Conference (WCNC '07)*, Las Vegas, Nev, USA, November 2007.

[27] M. Heidari and K. Pahlavan, "A model for dynamic behavior of ranging errors in TOA-based indoor geolocation systems," in *Proceedibgs of the 64th IEEE Vehicular Technology Conference (VTC '06)*, pp. 1–5, Montreal, QC, Canada, September 2006.

[28] I. Guvenc, C.-C. Chong, and F. Watanabe, "Joint TOA estimation and localization technique for UWB sensor network applications," in *Proceedings of the 65th IEEE Vehicular Technology Conference (VTC '07)*, pp. 1574–1578, Dublin, Ireland, April 2007.

[29] I. Guvenc and Z. Sahinoglu, "Threshold selection for UWB TOA estimation based on kurtosis analysis," *IEEE Communications Letters*, vol. 9, no. 12, pp. 1025–1027, 2005.

[30] J. Karedal, S. Wyne, P. Almers, F. Tufvesson, and A. F. Molisch, "A measurement-based statistical model for industrial ultrawideband channels," *IEEE Transactions on Wireless Communications*, vol. 6, no. 8, pp. 3028–3037, 2007.

[31] B. Alavi and K. Pahlavan, "Analysis of undetected direct path in time of arrival based UWB indoor geolocation," in *Proceedings of the 62nd IEEE Vehicular Technology Conference (VTC '05)*, vol. 4, pp. 2627–2631, Dallas, Tex, USA, September 2005.

[32] N. Alsindi, X. Li, and K. Pahlavan, "Performance of TOA estimation algorithms in different indoor multipath conditions," in *Proceedings of IEEE Wireless Communications and Networking Conference (WCNC '04)*, vol. 1, pp. 495–500, Atlanta, Ga, USA, March 2004.

[33] A. Leon-Garcia, *Probablity and Random Processes for Electrical Engineering*, Addison Wesley, Boston, Mass, USA, 2nd edition, 1994.

[34] H. V. Poor and X. Wang, "Code-aided interference suppression for DS/CDMA communications. Part II: parallel blind adaptive implementations," *IEEE Transactions on Communications*, vol. 45, no. 9, pp. 1112–1122, 1997.

[35] S. E. Bensley and B. Aazhang, "Maximum likelihood synchronization of a single user for code-divistion multiple access communication systems," *IEEE Transactions of Communications*, vol. 46, no. 3, pp. 392–399, 1998.

[36] A. H. Sayed, *Fundamentals of Adaptive Filtering*, John Wiley ' Sons, New York, NY, USA, 1st edition, 2003.

[37] Y.-H. Jo, J.-Y. Lee, D.-H. Ha, and S.-H. Kang, "Accuracy enhancement for UWB indoor positioning using ray tracing," in *IEEE/ION Position, Location, And Navigation Symposium*, vol. 2006, pp. 565–568, San Diego, Calif, USA, April 2006.

[38] N. A. Alsindi, B. Alavi, and K. Pahlavan, "Spatial characteristics of UWB TOA-based ranging in indoor multipath environments," in *IEEE International Symposium on Personal Indoor and Mobile Radio Communications (PIMRC '07)*, Athens, Greece, September 2007.

[39] B. Alavi and K. Pahlavan, "Modeling of the distance error for indoor geolocation," in *IEEE Wireless Communications and Networking Conference (WCNC '03)*, vol. 1, pp. 668–672, New Orleans, La, USA, March 2003.

[40] N. A. Alsindi, B. Alavi, and K. Pahlavan, "Measurement and modeling of UWB TOA-based ranging in indoor multipath environments," 2007, to appear in *IEEE Transactions on Vehicular Technology*.

[41] S. Markose and A. Alentorn, "The generalized extreme value (GEV) distribution, implied tail index and option pricing," Economics Discussion Papers 594, Department of Economics, University of Essex, Essex, UK, April 2005, http://ideas.repec.org/p/esx/essedp/594.html.

[42] K. P. Burnham and D. R. Anderson, *Model Selection and Multimodel Inference: A Practical Information-Theoretic Approach*, Springer, New York, NY, USA, 2nd edition, 2002.